



1 Article

6

10

11

13

14

15

16 17

19

21

- The Synthesis and Crystal Structure of Six Quaternary Lithi-
- 3 um-Alkaline Earth Metal Alumo-Silicides and Alu-
- mo-Germanides, A_2 LiAl Tt_2 (A = Mg, Ca, Sr, Ba; Tt = Si, Ge)
- 5 Paraskevi Kontomaris, Gregory M. Darone, Laura Camila Paredes Quevedo, and Svilen Bobev 3,*
 - ¹ Charter School of Wilmington, Wilmington, Delaware, United States
 - ² Universidad Nacional de Colombia, Bogota, Columbia
 - ³ Department of Chemistry and Biochemistry, University of Delaware, Newark, Delaware 19716, United States
 - * Correspondence: bobev@udel.edu; Tel.: +1-302-831-8720

Abstract: Reported are the synthesis and structural characterization of a series of quaternary lith-ium-alkaline earth metal alumo-silicides and alumo-germanides with the base formula $A_2\text{LiAl}Tt_2$ (A = Ca, Sr, Ba; Tt = Si, Ge). To synthesize each compound, a mixture of the elements with the desired stoichiometric ratio was loaded into a niobium tube, arc welded shut, enclosed in a silica tube under vacuum, and heated in a tube furnace. Each sample was analyzed by powder and single-crystal X-ray diffraction, and the crystal structure of each compound was confirmed and refined from single-crystal X-ray diffraction data. The structures, despite the identical chemical formulae are different, largely dependent on the nature of the alkaline earth metal. The differing cation determined the structure type; the calcium compounds are part of the TiNiSi family with the Pnma space group, the strontium compounds are isostructural with Na₂LiAlP₂ and have the Cmce space group, and the barium compounds crystallize with the PbFCl structure type in the P4/nmm space group. The anion (silicon or germanium) impacts only the size of the unit cell, with the silicides having smaller unit cell volumes than the germanides.

Keywords: lithium; germanium; silicon, solid-state structures, synthesis, Zintl phases

24

37

Citation: To be added by editorial 25 staff during production.

Academic Editor: Firstname Last- 27 name 28

Received: date
Accepted: date
Published: date

Publisher's Note: MDPI stays neu₃₃ tral with regard to jurisdictional 4 claims in published maps and insti-35 tutional affiliations.



Copyright: © 2022 by the author 39 Submitted for possible open access 40 publication under the terms and 41 conditions of the Creative Commons 42 Attribution (CC BY) license (https://creativecommons.org/license s/by/4.0/).

1. Introduction

Zintl phases typically contain electropositive cations (alkali, alkaline earth, or rare earth metals) and electronegative early p-block metals and semimetals from groups 13 to 15, which are the (poly)anions [1]. With climate change becoming increasingly dominant, switching from fossil fuels to sustainable energy sources and reducing global inefficiencies are main priorities. Since many Zintl phases are intrinsic semiconductors, they could be the bases for materials with applications in solid-state energy conversion and/or storage [2-7], which further sustainability.

In recent years, we have been studying the lithiation behavior of Si-, Ge-, and Sn-based clathrates [8-13]. In particular, over the course of our work with the type-I clathrates BasAl $_x$ Si $_{46-x}$ and BasAl $_x$ Ge $_{46-x}$ (0 < x < 16) [14-16], we observed the presence of some unknown phases as reaction byproducts. The latter were presumed to be new quaternary compounds with hitherto unknown structures and compositions. These observations were the motivation to create the following research plan for the summer internship; and so, the goal of this research was the rational synthesis of new Zintl phases comprising lithium and silicon or germanium. Hence, we set out to explore the A-Li-Al-Tt systems (A = Mg, Ca, Sr, Ba; Tt = Si, Ge) and our starting points were the equiatomic nominal compositions. The syntheses quickly yielded several new compounds in each respective system. Below, we detail the synthetic work that led to the identification of the title compounds, as well as describe their crystal structures. At the

61

62

63

66 67 68

77

78

79

80

81

outset, we draw attention to the fact that the structures, despite their same general chemical formula, are different (Figure 1). Each compound's differing anion (silicon or germanium) impacts only the size of the unit cell, with the silicides having smaller unit cell volumes than the germanides. The nature of the alkaline earth metal appears to influence which structure forms, with the calcium compounds being analogs of the TiNi-Si/SrMgSi family (Pnma space group); the strontium compounds being a part of the Na₂LiAlP₂ structural family (*Cmce* space group), and the barium compounds crystallizing with the PbFCl structure type in the tetragonal P4/nmm space group. Synthesis of Mg2LiAlSi2 and Mg2LiAlGe2 failed.

Several europium and ytterbium compounds were also synthesized. The characterization work is still ongoing and the results will be detailed in a later publication. We will just note that the europium compounds appear to mirror the crystal chemistry of the barium compounds, but the ytterbium compounds have differing structures and compositions. For that reason, the synthesized rare earth metal compounds are not included here.

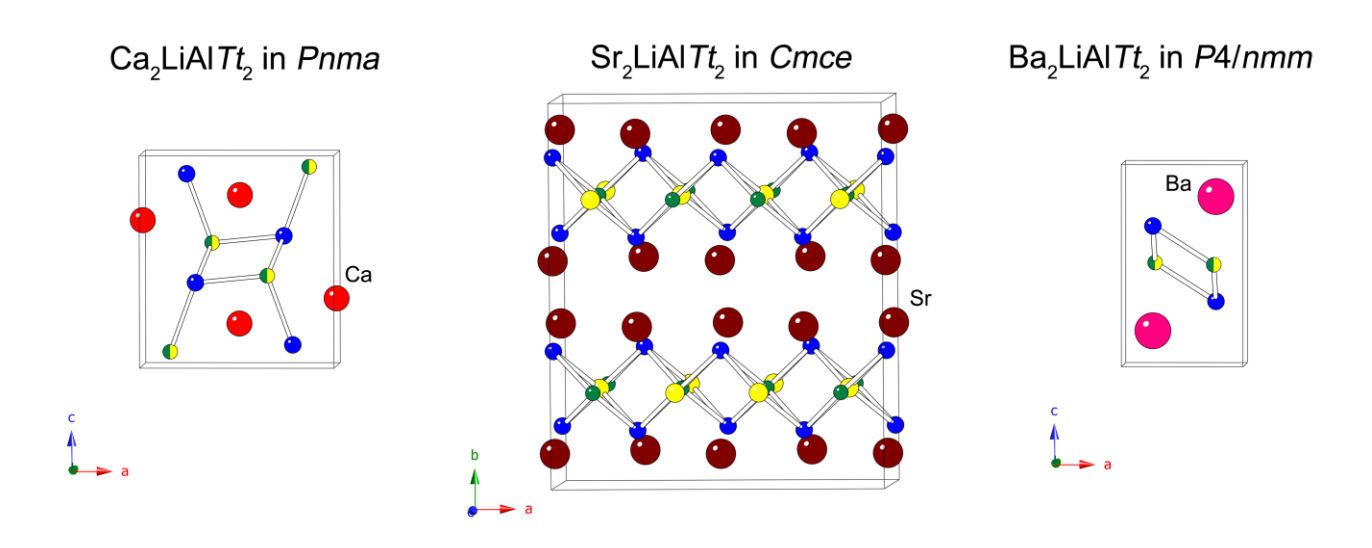


Figure 1. Schematic representation of the three types of crystal structures adopted by the $A_2\text{LiAl}Tt_2$ (A = Ca, Sr, Ba; Tt = Si, Ge) compounds. Green, yellow, and blue colors represent the Al, Li, and Ttatoms, respectively; mixed-occupied Al/Li positions are shown as two-tone. Ca, Sr, and Ba atoms can be distinguished by the light red, dark red and magenta spheres, respectively. Bonds (sticks) are drawn only between neighboring Al, Li, and *Tt* atoms. Unit cells are outlined.

2. Results

Crystal data for A_2 LiAl Tt_2 (A = Ca, Sr, Ba; Tt = Si, Ge) can be found in Tables 1, 2, and 3, respectively. We should note that our initial results from the system Ba-Li-Al-Ge, based on single-crystal X-ray diffraction work, showed the co-existence of Li and Al atoms on a single crystallographic site, which piqued our attention. Later on, the same result was replicated for the system Ba-Li-Al-Si. The Ca-compounds, although with a differing crystal structure, also showed Li and Al atoms on a single crystallographic site (Table 4). The refined chemical formulae in all 4 cases were $ALi_xAl_{1-x}Tt$ (A = Ca, Ba; Tt = Si, Ge) with $x \approx \frac{1}{2}$; however, subsequent synthetic work showed that changes in the nominal Li: Al ratio do not contribute to changes in the unit cell volume and there were no peak-shifts when experimental and simulated powder X-ray diffraction patterns were

109 110

111

112

113

114 115 116

105

106

107

108

compared. For the Sr-based compounds, Li and Al were found to occupy individual sites and were not disordered. Therefore, in this article, we labeled all six new alumo-silicides and alumo-germanides with the base formula $A_2\text{LiAl}Tt_2$ (A = Ca, Sr, Ba; Tt = Si, Ge), neglecting the arguably small possibility of trivial deviations from the stated stoichiometry.

As seen from Tables 1, 2, and 3 (as well as from Table 4, where the atomic coordinates of each of the 6 structures are given), there are three basic structures adopted by each the Ca-, Sr-, and Ba-compounds, respectively. All three types of structures (Figure 1) share a common feature—tetrahedral (or rather distorted tetrahedral) coordination of Al and Li atoms by the atoms of the Tt-element. In the case of the Ca- and Ba-compounds, there is no long-range ordering and the refined models have Li and Al atoms occupying the same crystallographic positions, while in the case of the Sr-compounds, there is no randomization and the derived crystal structures of Sr₂LiAlSi₂ and Sr₂LiAlGe₂ are devoid of disorder. Apparently, the packing of the Al Tt_4 and Li Tt_4 fragments together with the increasing size of the alkaline earth metal atom (in the expected order Ca < Sr < Ba) governs the formation of each structure, as it will be discussed in the next section. In that regards, we will mention that Mg2LiAlSi2 and Mg2LiAlGe2 were attempted to be synthesized using the same synthesis procedure (elements in the targeted stoichiometric ratio loaded into niobium tube, arc welded shut, enclosed in a silica tube under vacuum, and heated in tube furnaces according to the same heating profile as for the Ca-, Sr-, and Ba-counterparts). The resultant products were not the quaternaries Mg2LiAlSi2 and Mg2LiAlGe2. Instead, three different crystals could be identified with a naked eye: 1) blue, shiny gem-like crystals, 2) atmosphere-reactive silver crystals, and 3) dark, hard, brittle crystals. The blue crystals were determined to be cubic Mg2Si or Mg2Ge. The other crystals could not be identified reliably. We posit that Mg is either too small to form structures comparable to the Ca, Sr, and Ba compounds detailed in this paper, or may form covalent bonds with Al and the Tt-element. Reactions with the heavier congener of Si and Ge, Sn, were not explored as a part of this study.

Table 1. Selected crystallographic data for Ca₂LiAlSi₂ and Ca₂LiAlGe₂ (T = 200(2) K; Mo $K\alpha$, $\lambda = 0.71073$ Å, space group *Pnma* (no. 62)). Pearson symbol for this structure is oP12.

Chemical formula	Ca ₂ LiAlSi ₂	Ca ₂ LiAlGe ₂
fw/g mol ⁻¹	170.26	259.26
a /Å	7.2914 (7)	7.3255 (8)
b/Å	4.3411 (4)	4.3801 (5)
c /Å	7.9511 (8)	8.0246 (9)
$V/ m \AA^3$	251.67 (4)	257.48 (5)
$ ho_{ m calc.}/{ m g~cm^{-3}}$	2.25	3.34
$\mu_{(\text{Mo-K}_{lpha})}$ /cm ⁻¹	27.3	136.5
Collected reflections	1999	5187
Independent reflections	430	450
Goodness-of-fit	1.074	1.044
$R_1 (I > 2\sigma(I))^a$	0.0189	0.0287
$wR_2 (I > 2\sigma(I))^a$	0.0407	0.0535
R_1 (all data) ^a	0.0233	0.0361
wR_2 (all data) a	0.0417	0.0553
Δho max,min/ ${ m e}^{-}\cdot { m \mathring{A}}^{-3}$	0.38, -0.25	0.65, -0.76

^a $R_1 = \sum ||F_0| - |F_c||/\sum |F_0|$; $wR_2 = [\sum [w(F_0^2 - F_c^2)^2]/\sum [w(F_0^2)^2]]^{1/2}$, where $w = 1/[\sigma^2 F_0^2 + (AP)^2 + (BP)]$ and $P = (F_0^2 + 2F_c^2)/3$; A and B are the respective weight coefficients (see the CIFs).

Table 2. Selected crystallographic data for Sr₂LiAlSi₂ and Sr₂LiAlGe₂ (T = 200(2) K; Mo $K\alpha$, $\lambda = 0.71073$ Å, space group *Cmce* (no. 64)). Pearson symbol for this structure is oS48.

$Sr_2LiAlSi_2$	$Sr_2LiAlGe_2$
265.34	354.34
12.5283 (4)	12.616 (3)
14.4678 (7)	14.574 (3)
6.2735 (7)	6.3133 (3)
1137.1 (2)	1160.7 (4)
3.10	4.06
191.7	285.3
6957	4519
908	848
1.18	1.10
0.0263	0.0334
0.0434	0.0551
0.0388	0.0619
0.0464	0.0617
1.28, -0.72	1.27, -0.94
	265.34 12.5283 (4) 14.4678 (7) 6.2735 (7) 1137.1 (2) 3.10 191.7 6957 908 1.18 0.0263 0.0434 0.0388 0.0464

a $R_1 = \sum ||F_0| - |F_c||/\sum |F_0|$; $wR_2 = [\sum [w(F_0^2 - F_c^2)^2]/\sum [w(F_0^2)^2]]^{1/2}$, where $w = 1/[\sigma^2 F_0^2 + (AP)^2 + (BP)]$ and $P = (F_0^2 + 2F_c^2)/3$; A and B are the respective weight coefficients (see the CIFs).

Table 3. Selected crystallographic data for Ba₂LiAlSi₂ and Ba₂LiAlGe₂ (T = 200(2) K; Mo $K\alpha$, $\lambda = 0.71073$ Å, space group P4/nmm (no. 129)). Pearson symbol for this structure is tP6.

Chemical formula	Ba ₂ LiAlSi ₂	Ba ₂ LiAlGe ₂
fw /g mol ⁻¹	364.78	453.78
a /Å	4.5574 (6)	4.5965 (7)
c /Å	7.5582 (3)	7.5822 (7)
$V/ m \AA^3$	156.98 (4)	160.19 (5)
$ ho_{ m calc.}/ m g~cm^{-3}$	3.86	4.70
$\mu_{(\text{Mo-K}_{lpha})}$ /cm ⁻¹	128.4	214.1
Collected reflections	1309	1316
Independent reflections	172	170
Goodness-of-fit	1.108	1.099
$R_1 (I > 2\sigma(I))^a$	0.0167	0.0226
$wR_2 (I > 2\sigma(I))^a$	0.0339	0.0443
R_1 (all data) ^a	0.0194	0.0286
wR_2 (all data) a	0.0348	0.0456
$\Delta ho_{ m max,min} / e^- \cdot \mathring{A}^{-3}$	1.10, -0.71	0.95, -0.91
- D THE BUILD D	FEE (F.A. F.A.) O3 (TO F (TO O) O3 31 (O) 1

^a $R_1 = \sum ||F_0| - |F_c||/\sum |F_0|$; $wR_2 = [\sum [w(F_0^2 - F_c^2)^2]/\sum [w(F_0^2)^2]]^{1/2}$, where $w = 1/[\sigma^2 F_0^2 + (AP)^2 + (BP)]$ and $P = (F_0^2 + 2F_c^2)/3$; A and B are the respective weight coefficients (see the CIFs).

Table 4. Refined atomic coordinates for $A_2\text{LiAl}Tt_2$ (A = Ca, Sr, Ba; Tt = Si, Ge). In all cases, unless noted otherwise, the atoms are refined anisotropically and the values of their equivalent isotropic displacement parameters ($U_{\text{eq}}/\mathring{A}^2$) are given as well.

Ca ₂ LiAlSi ₂					
Atom	Wyckoff Site	x	y	z	$U_{ m eq}$ / $ m \AA^2$
Ca	4c	0.0100(1)	1/4	0.6907(1)	0.013(1)
Li/Al a	4c	0.1500(1)	1/4	0.0708(1)	0.012(1)
Si	4c	0.2802(1)	1/4	0.3960(1)	0.016(1)

Ca ₂ LiAlGe ₂					
Ca	4 <i>c</i>	0.0104(1)	1/4	0.6923(1)	0.014(1)
Li/Al a	4c	0.1500(1)	1/4	0.0704(3)	0.018(1)
Ge	4c	0.2780(1)	1/4	0.3959(1)	0.015(1)
		Sr ₂ Li	AlSi ₂		
Sr1	8 <i>e</i>	1/4	0.3349(1)	1/4	0.009(1)
Sr2	8 <i>f</i>	0	0.1634(1)	0.2283(1)	0.010(1)
Li	8 <i>d</i>	0.1254(7)	0	0	0.01 b
Al	8 <i>d</i>	0.3720(1)	0	0	0.012(1)
Si1	8 <i>e</i>	1/4	0.1028(1)	1/4	0.009(1)
Si2	8 <i>f</i>	0	0.3968(1)	0.2235(2)	0.010(1)
		Sr ₂ Li.	AlGe2		
Sr1	8 <i>e</i>	1/4	0.3352(1)	1/4	0.010(1)
Sr2	8 <i>f</i>	0	0.1634(1)	0.2294(1)	0.011(1)
Li	8 <i>d</i>	0.1257(5)	0	0	0.01^{b}
Al	8 <i>d</i>	0.3726(1)	0	0	0.015(1)
Ge1	8 <i>e</i>	1/4	0.1047(1)	1/4	0.009(1)
Ge2	8 <i>f</i>	0	0.3951(1)	0.2276(1)	0.010(1)
	Ba ₂ LiAlSi ₂				
Ва	2 <i>c</i>	1/4	1/4	0.6732(1)	0.018(1)
Li/Al a	2 <i>a</i>	3/4	1/4	0	0.015(1)
Si	2 <i>c</i>	1/4	1/4	0.1914(3)	0.020(1)
Ba ₂ LiAlGe ₂					
Ва	2 <i>c</i>	1/4	1/4	0.6743(1)	0.016(1)
Li/Al a	2 <i>a</i>	3/4	1/4	0	0.016(1)
Ge	2 <i>c</i>	1/4	1/4	0.1953(1)	0.018(1)
	a Rofined or	cumancies were cons	trained to be Li · A	$1 = 50 \cdot 50$ b Rofin	ed isotropically (11-

^a Refined occupancies were constrained to be Li : Al = 50 : 50. ^b Refined isotropically ($U_{eq} = U_{iso}$) and with value constrained to the average U_{eq} value for the heavy atoms in the structure.

In summary, the reaction method detailed in this paper, with or without significant deviations, may produce more $A_2\text{LiAl}Tt_2$ (A = Mg, Yb; Tt = Si, Ge, Sn) compounds, but further inquiries must be made.

3. Discussion

We begin the discussion with the structure of Ca₂LiAlSi₂ and Ca₂LiAlGe₂, which crystallize with the orthorhombic space group *Pnma* (no. 62). They are isotypic with Ti-NiSi (Pearson symbol *oP*12) structure type; the structure has three unique positions in the asymmetric unit. As such, and as described previously, Li and Al atoms are considered to be statistically disordered.

A schematic representation of the structure is given in Figure 2. The chosen view shows that the structure can be viewed as a 3D-network made up of edge- and corner-shared tetrahedra (Al Tt_4 and Li Tt_4), with the Ca atoms taking the space within the created channels. The tetrahedral units are slightly distorted from the ideal geometry and have two shorter and two longer Li/Al-Tt bonds. The respective distances are tabulated in Table 5.

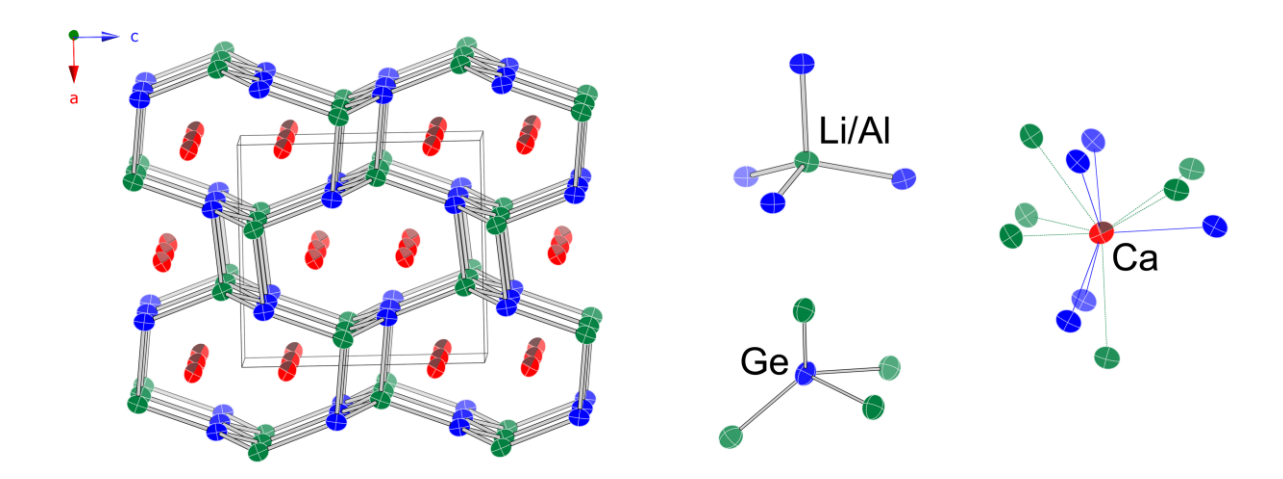


Figure 2. Schematic representation of the orthorhombic crystal structure of Ca₂LiAlGe₂ (TiNi-Si/SrMgSi structure type, space group *Pnma*). Green, blue and red colors represent Al/Li, Ge and Ca atoms, respectively. Anisotropic displacement parameters are drawn at the 95% probability level. Unit cell is outlined

Table 5. Selected interatomic distances (Å) in Ca₂LiAlSi₂ and Ca₂LiAlGe₂.

Ca ₂ LiAlSi ₂		Ca ₂ LiAlGe ₂		
Atom pair	Distance/ Å	Atom pair	Distance/ Å	
Si—Li/Al	2.709 (1)	Ge-Li/Al	2.736 (3)	
Si—Li/Al	2.754 (1)	Ge-Li/Al	2.776 (3)	
$Si-Li/Al \times 2$	2.6272 (6)	$Ge-Li/Al \times 2$	2.653 (2)	
Ca-Li/Al	3.190(1)	Ca—Li/Al	3.201 (3)	
$Ca-Li/Al \times 2$	3.1093(7)	$Ca-Li/Al \times 2$	3.130 (2)	
Ca-Li/Al	3.349 (1)	Ca-Li/Al	3.381 (3)	
$Ca-Li/Al \times 2$	3.4301 (7)	$Ca-Li/Al \times 2$	3.458 (2)	
Ca-Si	3.0615 (7)	Ca—Ge	3.082 (1)	
$Ca-Si \times 2$	3.1089(5)	Ca-Ge × 2	3.1242 (7)	
$Ca-Si \times 2$	3.1168 (5)	Ca—Ge×2	3.1414 (8)	
$Li/Al-Si \times 2$	2.6272 (6)	$Li/Al-Ge \times 2$	2.653 (2)	
Li/Al—Si	2.709 (1)	Li/Al—Ge	2.735 (3)	
Li/Al—Si	2.754 (1)	Li/Al—Ge	2.776 (3)	

Four-fold coordination environments exist around the Si and Ge atoms too, but in that case, the distortions from the ideal tetrahedral angle, in particular, are more severe. Si—Li/Al and Ge—Li/Al distances are about 10% longer than the sum of the single-bonded Pauling covalent radii (r_{Li} = 1.225 Å; r_{Al} = 1.248 Å; r_{Si} = 1.173 Å; r_{Ge} = 1.242 Å) [17]. These distances match the reported values in a number of alumo-silicides and alumo-germanides, such as LiAlSi [18], LiAlGe [19], CaAl₂Si₂ [20], Ca₃Al₂Ge₂ [21], SrAl₂Ge₂ [22], BaAl₂Si₂ [23], Ln_2 Al₃Si₂ and Ln_2 Al₃Ge₄ (Ln = lanthanide) [24-26], among others. Ca

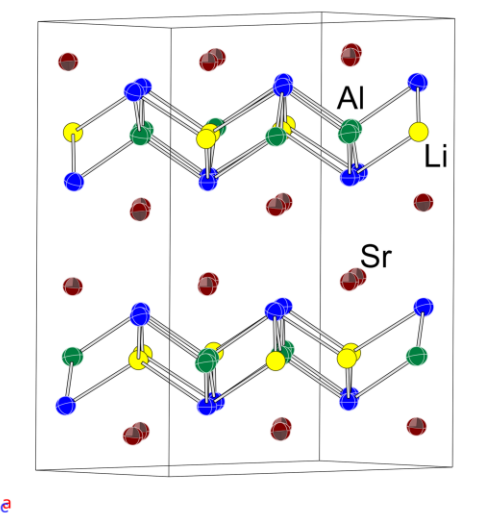
atoms have a total coordination number 11, with 6 nearest Li/Al and 5 nearest Tt atoms. The shortest contact is $d_{Ca-Si} = 3.06$ Å, which also matches fairly closely the sum of the single-bonded Pauling covalent radii of Si and Ca ($r_{Ca} = 1.736$ Å).

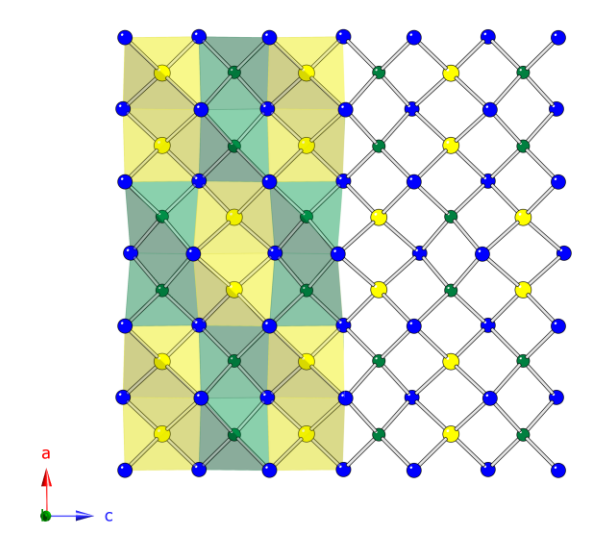
In the fully ionic approximation, the structures of Ca₂LiAlSi₂ and Ca₂LiAlGe₂ can be rationalized as $(Ca^{2+})_2(Li^+)(Al^{3+})(Si^4-)_2$ and $(Ca^{2+})_2(Li^+)(Al^{3+})(Ge^4-)_2$, i.e., the compounds should be considered intrinsic semiconductors. Applying the Zintl concept [1] also leads to the same conclusion—when treating Li as a cation and Al as a part of the polyanionic 4-bonded substructure, it becomes possible to partition the valence electrons the following way: $(Ca^{2+})_2(Li^+)(4b-Al^{1-})(4b-Si^0)(0b-Si^{4-})$ and $(Ca^{2+})_2(Li^+)(4b-Al^{1-})(4b-Ge^0)(0b-Ge^{4-})$. To arrive at this formula breakdown, we are assuming covalent Si—Al and Ge—Al interactions; Si and Al are coordinated to Al atoms 50% of the time. In the remaining 50% of the time, Li is taking the Al position and covalency of the Si—Li and Ge—Li is neglected, i.e., Si and Ge are treated as isolated, closed-shell anions.

Following periodic trends, the structure of Sr₂LiAlSi₂ and Sr₂LiAlGe₂ will be discussed next. These compounds are also orthorhombic, but with the base-centered space group *Cmce* (no. 64). They are isotypic with Na₂LiAlP₂ (Pearson symbol *oS*48) and the structure has six unique positions in the asymmetric unit—two for the Sr atom, two for the Si or Ge atoms, and one each for the Li and Al atoms, Table 4. As such, and as described previously, this is the only "true 2-1-1-2" structure since Li and Al atoms are ordered crystallographically here.

A schematic representation of the structure is given in Figure 3. The chosen view shows that the structure can be viewed as slabs made up of all edge-shared $AlTt_4$ and $LiTt_4$ tetrahedra parallel to the *ac*-plane. The general topology of the 2D-polyanionic substructure is reminiscent of the PbO-like layers that are frequently observed in the structures of many pnictides and chalcogenides [27], and analogous to the layers seen in the tetragonal structures of $Ba_2LiAlSi_2$ and $Ba_2LiAlGe_2$, which will be discussed next. The difference is that here, since there is no Li/Al disorder, the exact positions of Li and Al atoms are known and the ordering pattern is checkerboard-like with a repeating sequence $AlTt_4 \times 2$ by $LiTt_4 \times 2$ (Figure 3, right panel).

The Al Tt_4 and Li Tt_4 tetrahedral units are ever so slightly distorted from the ideal geometry and have two shorter and two longer Li/Al-Tt bonds. The refined bond lengths matching well the sum of the single-bonded Pauling covalent radii of the elements. Sr atoms are arranged in double layers between the [LiAlSi2] and [LiAlGe2] slabs. They have a total coordination number 9, with 5 nearest Tt atoms, 2 nearest Al, and 2 neighboring Li atoms. All respective distances are tabulated in Table 6.





216

217 218

219

220

221

222

223

224 225

226

Figure 3. (left panel) Schematic representation of the orthorhombic crystal structure of Sr₂LiAlGe₂ (Na₂LiAlP₂ structure type, space group *Cmce*). The chosen projection is to highlight the similarity to another structure, and the unit cell is outlined. Green, yellow, blue, and red colors represent the Al, Li, Ge, and Sr atoms, respectively. Anisotropic displacement parameters are drawn at the 95% probability level. (right panel) A projection of a single [LiAlGe2] slab, viewed down the b-axis. The checkerboard-like pattern of all edge-shared tetrahedra is emphasized.

Table 6. Selected interatomic distances (Å) in Sr₂LiAlSi₂ and Sr₂LiAlGe₂.

- Table 6. Science	a interatorne dist	arices (71) III 512E111	1312 and 312LIAIGe2.
Sr ₂ LiA	1Si ₂	Sr ₂ Li	AlGe2
Atom pair	Distance/ Å	Atom pair	Distance/ Å
$Si1-Al \times 2$	2.647 (1)	$Ge1-Al \times 2$	2.686 (2)
$Si1-Li \times 2$	2.666 (5)	$Ge1-Li \times 2$	2.70 (1)
$Si2-Al \times 2$	2.600(1)	$Ge2-Al \times 2$	2.643 (2)
$Si2-Li \times 2$	2.775 (5)	Ge2—Li×2	2.79 (1)
	2 2 4 1 2 (0)		2.2 (4.42)
$Sr1-Al \times 2$	3.2413 (9)	$Sr1-Al \times 2$	3.264 (2)
$Sr1-Li \times 2$	3.257 (4)	$Sr1-Li \times 2$	3.275 (9)
$Sr1-Si1 \times 2$	3.2639 (5)	$Sr1-Ge1 \times 2$	3.2758 (7)
Sr1—Si1	3.358 (2)	Sr1—Ge2	3.360 (2)
$Sr1-Si2 \times 2$	3.2621 (5)	$Sr1-Ge2 \times 2$	3.2756 (7)
$Sr2-Al \times 2$	3.3260 (9)	$Sr2-Al \times 2$	3.343 (2)
$Sr2-Li \times 2$	3.179 (5)	$Sr2-Li \times 2$	3.206 (9)
$Sr2-Si1 \times 2$	3.2554 (5)	$Sr2-Ge1 \times 2$	3.2706 (7)
Sr2-Si2	3.226 (1)	Sr2-Ge2	3.2585 (6)
Sr2-Si2	3.285 (1)	Sr2-Ge2	3.281 (1)
Sr2—Si2	3.378 (2)	Sr2—Ge2	3.377 (2)
$Al-Si1 \times 2$	2.647 (1)	Al—Ge1 × 2	2.686 (2)
$A1-Si2 \times 2$	2.600 (1)	$Al-Ge2 \times 2$	2.643 (2)
$Li-Si1 \times 2$	2.666 (5)	$Li-Ge1 \times 2$	2.70 (1)
$Li-Si2 \times 2$	2.775 (5)	$Li-Ge2 \times 2$	2.79 (1)

The application of the Zintl concept here [1] is more instructive than what we considered before on the examples of Ca₂LiAlSi₂ and Ca₂LiAlGe₂, since no disorder is present and no assumptions need to be made. Hence, using the same scheme to partition the vapropose the following formulae electrons, we can $(Sr^{2+})_2(Li^+)(4b-Al^{1-})(2b-Si^{2-})_2$ and $(Sr^{2+})_2(Li^+)(4b-Al^{1-})(2b-Ge^{2-})_2$. To arrive at them, only Si-Al and Ge-Al interactions were treated as covalent. In a more extreme case, where Si-Li and Ge-Li bonds are also treated as covalent, all Tt atoms will be four-bonded and will bear no formal charge. Li with 4 covalent bonds must be considered as formally, 4b-Li3-, in analogy with the Zintl clathrate Ba8Li5Ge41 [5]. In this scenario, the valence electron count can be ascribed as follows: (Sr²⁺)₂(4b-Li³⁻)(4b-Al¹⁻)(4b-Si⁰)₂ and $(Sr^{2+})_2(4b-Li^{3-})(4b-Al^{1-})(4b-Ge^0)_2$.

The last remaining structure to briefly discuss is that of Ba₂LiAlSi₂ and Ba₂LiAlGe₂. The latter two compounds crystallize with the tetragonal space group *P*4/*nmm* (no. 129). This is a structure type known as PbFCl (Pearson symbol *tP*6), which is very common and well known (Figure 4). There are three unique positions in the asymmetric unit (Table 4), meaning that Li and Al atoms are, again, statistically disordered.

From the schematic representation of the structure in Figure 4, it is evident that the overall arrangement of the atoms is nearly identical to that described above for the orthorhombic $Sr_2LiAlSi_2$ and $Sr_2LiAlGe_2$; the major difference is that the ordering of the tetrahedral $AlTt_4$ and $LiTt_4$ units is averaged in this symmetry. The Ba atoms take the space between the layers and have the exact same coordination environment (CN 9) as the Sr atoms in $Sr_2LiAlSi_2$ and $Sr_2LiAlGe_2$ (*vide supra*). Another Si atom is 3.9 Å away, i.e., is the topmost Si atom in Figure 4, for which a line denoting Si—Ba contact is not drawn.

Naturally, since Ba is the largest element from group 2, all distances here are slightly longer compared to the Ca- and Sr-based compounds. Specifically, the average bond lengths A-Al and A-Li (A = Ca, Sr, Ba) in Ca₂LiAl Tt_2 , Sr₂LiAl Tt_2 and Ba₂LiAl Tt_2 (Tt = Si, Ge) increase as the differing cation increases in size. In other words, the average A-Al and A-Li contact in Ca₂LiAlSi₂ are shorter than those in Sr₂LiAlSi₂, which are in turn shorter than those in Ba₂LiAlSi₂. The same principle applies to the analogous germanides. For example, for the silicides, the average Ca-Al/Li distance is 3.14 Å, whereas the average Ba-Al/Li is 3.36 Å (recall that both structures have Al and Li atoms disordered).

Of note is also the fact that the 4-fold symmetry in $Ba_2LiAlTt_2$ makes the tetrahedral units much closer to the ideal geometry, as they have four equal Li/Al-Tt bonds. Ge coordination environment is square-pyramidal. All respective distances are tabulated in Table 7.

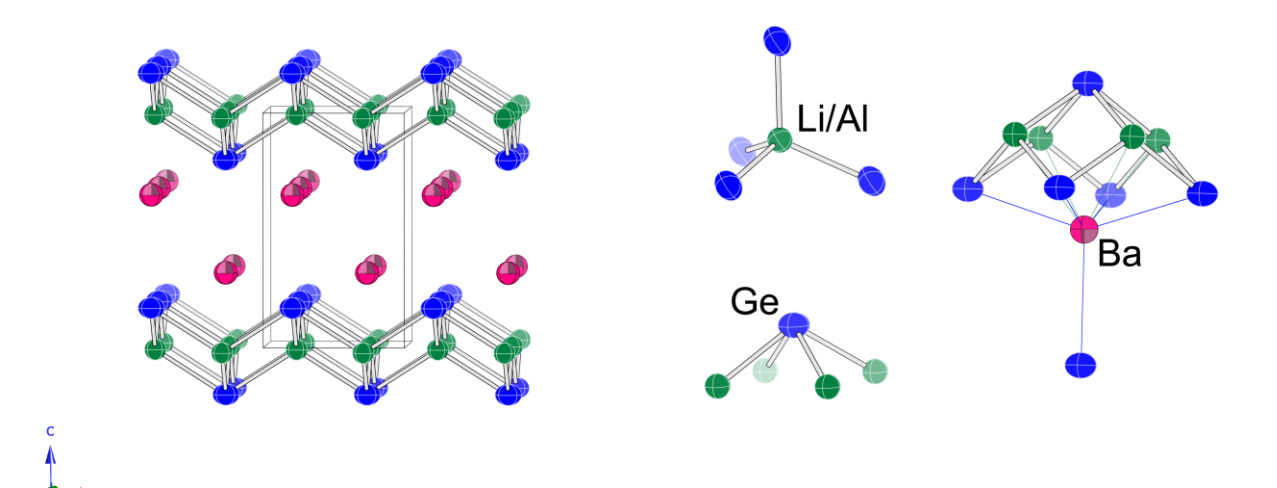


Figure 4. (left panel) Schematic representation of the orthorhombic crystal structure of Ba₂LiAlGe₂ (PbFCl structure type, space group *P4/nmm*). Green, blue, and magenta colors represent the Al/Li, Ge, and Ba atoms, respectively. Anisotropic displacement parameters are drawn at the 95% probability level.

Table 7. Selected interatomic distances (Å) in Ba2LiAlSi2 and Ba2LiAlGe2.

Ba ₂ LiAlSi ₂		Ba ₂ LiAlGe ₂		
Atom pair	Distance/ Å	Atom pair	Distance/ Å	

	Du 11/111 × 1	0.0007 (0)	Du 11/111 \ 1	0.0700 (7)
	$Ba-Si \times 4$	3.3812 (7)	$Ba-Ge \times 4$	3.3974 (6)
	Ba—Si	3.641 (2)	Ba-Ge	3.632 (2)
	$Si-Li/Al \times 4$	2.6992 (1)	Ge-Li/Al × 4	2.7340 (7)
	Li/Al—Si × 4	2.6992 (1)	$Li/Al-Ge \times 4$	2.7340 (7)
260				
261				
262	Just like	with the cases	of Ca ₂ LiAlTt ₂ and	$Sr_2LiAlTt_2$, in
263	tion, the st	ructures of	Ba ₂ LiAlSi ₂ and	Ba ₂ LiAlGe ₂
	/D 2.\ /T 1.\ / A 12	.\(C'()\ 1 (D	2.) /T 1.) / A 12.) / C /)	

in the fully ionic approximacan be rationalized as $(Ba^{2+})_2(Li^+)(Al^{3+})(Si^{4-})_2$ and $(Ba^{2+})_2(Li^+)(Al^{3+})(Ge^{4-})_2$.

3.3738(7)

3.3607 (5) $B_a = Li/A1 \times 4$

4. Materials and Methods

4.1. Synthesis

 $Ba-Li/Al \times 4$

Objective: To synthesize and establish the structure of a series of novel quaternary alkaline earth metal and rare earth metal silicides and germanides, with the base formula A_2 LiAl Tt_2 (A = Mg, Ca, Sr, Ba, Eu, Yb; Tt = Si, Ge). For this purpose, given that Li and most of the alkaline earth metals are reactive towards air and moisture, all synthetic and post-synthetic manipulations were performed inside an argon-filled glove box or under vacuum.

All metals were used as received from Alfa or Aldrich (>99.9% wt.), except for Ba and Li, whose surfaces had to be carefully cleaned with a blade each time the metal rods were cut. In a typical experiment, a mixture of elements with the desired stoichiometric ratio (total weight ca. 500 mg) was loaded into a Nb tube, which was then sealed by arc-welding under an Ar atmosphere. The welded Nb tube was subsequently enclosed in a fused silica tube, which was flame-sealed under vacuum (below discharge).

To synthesize A2LiAlSi2 and A2LiAlGe2, the tubes with the reactant mixtures inside were heated in tube furnaces to 1223 K (rate of 300 K/h) and equilibrated for 8 h, followed by a cooling to 573 K at a rate of 200 K/h. The tubes were rotated in the furnaces at temperatures > 973 K. At the completion of their heat-treatment, all tubes were quenched in cold water. The products of this method were not phase pure.

Note: Many of the compounds detailed in this paper react rapidly with air and/or moisture. Corresponding with periodic trends, the germanides are more reactive than the silicide compounds. Moreover, the compounds' reactivity can be represented as $Ca_2LiAlTt_2 < Sr_2LiAlTt_2 < Ba_2LiAlTt_2$. $A_2LiAlGe_2$ (A = Ca, Sr, Ba) samples reacted with the ambient air and turned opaquely yellow within a few minutes. The A2LiAlSi2 samples experienced no visible color changes, but were not air stable beyond one hour, even when covered under an oil film. In direct contact with deionized water, both A2LiAlSi2 and A2LiAlGe2 ignited and volatilized.

4.2. Crystallographic Studies

Powder X-ray diffraction (PXRD) measurements were carried out at room temperature on a Rigaku Miniflex diffractometer (filtered Cu $K\alpha$ radiation, λ = 1.5418 Å). Small portions of the obtained samples were ground into powder using agate mortars and pestles inside the argon-filled glovebox. The specimens for PXRD were prepared by covering the polycrystalline material with a light film of oil and were transferred to another glovebox, which houses the diffractometer. The data were collected as quickly as possible with a typical θ - θ scan of 0.05°/step and data acquisition rate of 2 s/step. The collected powder X-ray diffraction patterns were used for phase identification of the reaction products only.

265 266

267 268 269

278

287

288

303

The PXRD measurements before and after exposure to air over confirmed the previously stated instability in air.

Single-crystal X-ray diffraction data for the six compounds were collected at 200 K using a Bruker SMART CCD-based diffractometer (three-circle goniometer; monochromated Mo $K\alpha$ radiation (λ = 0.710 73 Å)). First, several crystals from each batch were selected and checked before the best ones were chosen for intensity data collection. The experiments were managed in batch runs consisting of an appropriate number of frames to ensure 98% coverage in angular range in 20 of up to ca. 60° (frame width was typically 0.5-0.6° in ω and θ with a data acquisition rate of 6–8 s/frame). Data processing was done with the Bruker supplied software. SADABS was used for semi-empirical absorption correction based on equivalents [28]. The structure factors were sorted and merged by the subprogram XPREP in the SHELXTL software package [29], which was also employed in the space group determination. The structures were solved by direct methods and refined to convergence by full-matrix least-squares methods on F^2 . Selected details of the data collection and relevant crystallographic parameters of are given in Tables 1–4. Refined distances are tabulated in Tables 5–7.

Author Contributions: Conceptualization, S.B.; methodology, P.K., L.P., G.D.; data curation, P.K., L.P., G.D.; validation, P.K., L.P., G.D. and S.B.; formal analysis, S.B.; investigation, P.K., L.P., G.D.; resources, S.B.; writing—original draft preparation, P.K.; writing—conceptualization, P.K., S.B.; writing—review and editing, S.B.; visualization, S.B.; supervision, S.B.; project administration, S.B.; funding acquisition, S.B. All authors have read and agreed to the published version of the manuscript.

Funding: This work was supported by the US National Science Foundation (NSF) through grant DMR-2004579.

Data Availability Statement: The corresponding crystallographic information files (CIF) have been deposited with the Cambridge Crystallographic Database Centre (CCDC) and can be obtained free of charge via http://www.ccdc.cam.ac.uk/conts/retrieving.html (or from the CCDC, 12 Union Road, Cambridge CB2 1EZ, UK; Fax: +44-1223-336033; E-mail: deposit@ccdc.cam.ac.uk) with the following depository numbers: 2285060–2285065.

Acknowledgments: The authors thank Dr. T.-S. You for early exploratory work in the Ca–Li–Al–Ge system and Dr. M. O. Ogunbunmi for help with single-crystal X-ray diffraction data. P.K. gives thanks to Mrs. Jennifer Toner and Dr. Konstantinos Kontomaris for their exceptional guidance and encouragement throughout this project.

Conflicts of Interest: The authors declare no conflict of interest.

References

- 1. Nesper, R. The Zintl-Klemm Concept a Historical Survey. Z. Anorg. Allg. Chem. 2014, 640 (14), 2639–2648. https://doi.org/10.1002/zaac.201400403.
- 2. Toberer, E. S.; May, A. F.; Snyder, G. J. Zintl Chemistry for Designing High Efficiency Thermoelectric Materials. Chem. Mater. 2010, 22 (3), 624–634. https://doi.org/10.1021/cm901956r.
- 347 3. Kauzlarich, S. M.; Brown, S. R.; Snyder, G. J. Zintl Phases for Thermoelectric Devices. Dalton Trans. 2007, 21, 2099. https://doi.org/10.1039/b702266b.
- 4. Ogunbunmi, M. O.; Bobev, S. Exploiting the Fraternal Twin Nature of Thermoelectrics and Topological Insulators in Zintl Phases as a Tool for Engineering New Efficient Thermoelectric Generators. J. Mater. Chem. C 2023, 11 (25), 8337–8357. https://doi.org/10.1039/D3TC00556A.
 - 5. Kauzlarich, S. M. Special Issue: Advances in Zintl Phases. Materials 2019, 12 (16), 2554. https://doi.org/10.3390/ma12162554.
- 353 6. Snyder, G. J.; Toberer, E. S. Complex Thermoelectric Materials. Nature Mater. 2008, 7 (2), 105–114. 354 https://doi.org/10.1038/nmat2090.

367

368

383

- 55 7. Shi, X.-L.; Zou, J.; Chen, Z.-G. Advanced Thermoelectric Design: From Materials and Structures to Devices. Chemical Reviews 2020, 120 (15), 7399–7515. https://doi.org/10.1021/acs.chemrev.0c00026.
- 8. Ghosh, K.; Ovchinnikov, A.; Baitinger, M.; Krnel, M.; Burkhardt, U.; Grin, Y.; Bobev, S. Lithium Metal Atoms Fill Vacancies in the Germanium Network of a Type-I Clathrate: Synthesis and Structural Characterization of BasLisGe41. Dalton Trans. 2023, 52, 10310–10322. https://doi.org/10.1039/D3DT01168B.
- 9. Dopilka, A.; Weller, J. M.; Ovchinnikov, A.; Childs, A.; Bobev, S.; Peng, X.; Chan, C. K. Structural Origin of Reversible Li Insertion in Guest-Free, Type-II Silicon Clathrates. Adv. Energy Sust. Res. 2021, 2 (5), 2000114–2000114. https://doi.org/10.1002/aesr.202000114.
- Dopilka, A.; Childs, A.; Ovchinnikov, A.; Zhao, R.; Bobev, S.; Peng, X.; Chan, C. K. Structural and Electrochemical Properties of Type VIII Ba_δGa_{16-δ}Sn_{30+δ} Clathrate (δ ≈ 1) during Lithiation. ACS Appl. Mater. Interfaces 2021, 13 (36), 42564–42578. https://doi.org/10.1021/acsami.1c07240.
 - 11. Dopilka, A.; Ovchinnikov, A.; Childs, A.; Bobev, S.; Peng, X.; Chan, C. K. Understanding the Li and Na Intercalation in Si Clathrate Frameworks. In the proceedings of the 240th ECS Meeting, October 2021: IOPscience. https://iopscience.iop.org/article/10.1149/MA2021-022226mtga.
- 12. Dopilka, A.; Childs, A.; Bobev, S.; Chan, C. K. Electrochemical Lithium Alloying Behavior of Guest-Free Type II Silicon Clathrates. J. Phys. Chem. C 2021, 125 (35), 19110–19118. https://doi.org/10.1021/acs.jpcc.1c04020.
- 371 13. Dopilka, A.; Childs, A.; Bobev, S.; Chan, C. K. Understanding the Amorphous Lithiation Pathway of the Type I Ba₈Ge₄₃
 372 Clathrate with Synchrotron X-Ray Characterization. Chem. Mater. 2020, 32 (21), 9444–9457.
 373 https://doi.org/10.1021/acs.chemmater.0c03641
- 14. Dopilka, A.; Zhao, R.; Weller, J. M.; Bobev, S.; Peng, X.; Chan, C. K. Experimental and Computational Study of the Lithiation of BasAl_yGe_{46-y} Based Type I Germanium Clathrates. ACS Appl. Mater. Interfaces, 2018, 10 (44), 37981–37993. https://doi.org/10.1021/acsami.8b11509.
- 15. Li, Y.; Raghavan, R.; Wagner, N.; Davidowski, S. K.; Loïc Baggetto; Zhao, R.; Cheng, Q.; Yarger, J. L.; Veith, G. M.; Ellis-Terrell, C.; Miller, M. A.; Chan, K. S.; Chan, C. K. Type I Clathrates as Novel Silicon Anodes: An Electrochemical and Structural Investigation. Adv. Sci. 2015, 2 (6), 1500057–1500057. https://doi.org/10.1002/advs.201500057.
- 380 16. Zhao, R.; Bobev, S.; Krishna, L.; Yang, T.; Weller, J. M.; Jing, H.; Chan, C. K. Anodes for Lithium-Ion Batteries Based on Type I 381 Silicon Clathrate BasAl₁₆Si₃₀ - Role of Processing on Surface Properties and Electrochemical Behavior. ACS Appl. Mater. Interfaces, 2017, 9 (47), 41246–41257. https://doi.org/10.1021/acsami.7b12810.
 - 17. Pauling, L. The Nature of the Chemical Bond; Cornell University Press: Ithaca, NY, 1960.
- 18. Kevorkov, D.; Gröbner, J.; Schmid-Fetzer, R. The Al–Li–Si System: 1. A New Structure Type Li₈Al₃Si₅ and the Ternary Solid-State Phase Equilibria. J. Solid State Chem. 2001, 156 (2), 500–505. https://doi.org/10.1006/jssc.2000.9030
- 386 19. Gulebaglan, S. E.; Dogan, E. K. Prediction the Structural, Electronic, Elastic and Dynamical Properties of LiAlGe and LiInGe 387 Half-Heusler Crystals by Density Functional Theory. Mater. Today Commun. 2022, 32, 104082. 388 https://doi.org/10.1016/j.mtcomm.2022.104082
- 20. Zheng, C.; Hoffmann, R.; Nesper, R.; von Schnerring, H.-G. Site Preferences and Bond Length Differences in CaAl₂Si₂-Type Zintl Compounds. J. Amer. Chem. Soc. 1986, 108 (8), 1876–1884. https://doi.org/10.1021/ja00268a027.
- Widera, A.; Eisenmann, B.; Schäfer, H.; Turban, K. Darstellung und Kristallstruktur von Ca₃Al₂Ge₂, Sr₃Al₂Ge₂ und Ba₃Al₂Ge₂ / Preparation and Crystal Structure of Ca₃Al₂Ge₂, Sr₃Al₂Ge₂ and Ba₃Al₂Ge₂. Z. Naturforsch B 1976, 31, (12), 1592–1595. https://doi.org/10.1515/znb-1976-120.
- Suen, N.-T.; Bobev, S. Structures of Three Alkaline-Earth Metal Germanides Refined from Single-Crystal X-Ray Diffraction
 Data. Chemistry 2022, 4 (4), 1429–1438. https://doi.org/10.3390/chemistry4040094.
- 23. Condron, C. L.; Hope, H.; Paula; Schultz, A. J.; Kauzlarich, S. M. Synthesis, Structure, and Properties of BaAl₂Si₂. Inorg. Chem. 2007, 46 (11), 4523–4529. https://doi.org/10.1021/ic070078h.
- 398 24. Bobev, S.; Tobash, P. H.; Fritsch, V.; Thompson, J. D.; Hundley, M. F.; Sarrao, J. L.; Fisk, Z. Ternary Rare-Earth Alumo-Silicides—Single-Crystal Growth from al Flux, Structural and Physical Properties. J. Solid State Chem. 2005, 178 (6), 2091–2103. https://doi.org/10.1016/j.jssc.2005.04.021.
- 401 25. Tobash, P. H.; Bobev, S. The Structure of Ce₂Al₃Ge₄ Refined for the First Time from Single-Crystal X-Ray Diffraction Data. Acta
 402 Crystallogr. C 2021, 77 (2), 81–83. https://doi.org/10.1107/S2053229621000383.
- 403 26. Pearson, W. B. Pearson's Handbook of Crystallographic Data for Intermetallic Phases; American Society for Metals: Metals 404 Park, OH, 1985.
- 405 27. Ovchinnikov, A.; Bobev, S. Zintl Phases with Group 15 Elements and the Transition Metals: A Brief Overview of Pnictides with Diverse and Complex Structures. J. Solid State Chem. 2019, 270, 346–359. https://doi.org/10.1016/j.jssc.2018.11.029.
- 407 28. SADABS NT, version 2.10; Bruker Analytical X-ray Systems, Inc.: Madison, WI, 2001.
- 408 29. SHELXTL, version 6.12; Bruker Analytical X-ray Systems, Inc.: Madison, WI, 2001.